Radar and Optical Study of Defunct GEO Satellites

Conor J. Benson[a], Charles J. Naudet[b], Daniel J. Scheeres[a], Joseph S. Jao[b], Lawrence G. Snedeker[c], William H. Ryan[d], Eileen V. Ryan[d], Marc A. Silva[c], and Jeffrey K. Lagrange[c]

[a] University of Colorado Boulder, 3775 Discovery Drive, Boulder, CO 80309
[b] Jet Propulsion Laboratory, 4800 Oak Grove Drive, Pasadena, CA 91109
[c] Goldstone Deep Space Communications Complex, Fort Irwin, CA 92310
[d] Magdalena Ridge Observatory, New Mexico Tech, 101 East Road, Socorro, NM 87801

ABSTRACT

Understanding and predicting the evolving spin states of defunct GEO satellites and rocket bodies is important for space situational awareness, active debris removal, satellite servicing, anomaly resolution, and small asteroid evolution. There is clear evidence that many defunct GEO satellite spin states are predominantly driven by the Yarkovsky-O'Keefe-Radzievskii-Paddack (YORP) effect. The YORP effect is spin state evolution due to solar radiation and thermal re-emission torques. Observations are crucial to understand how YORP drives spin states and to validate dynamical models. Unfortunately, extracting spin states (spin periods, rotational angular momentum vector, instantaneous attitude) from ubiquitous photometric light curve data is challenging because GEO satellites are non-resolved from ground-based telescopes. Even for well-known objects, light curve inversion often yields several or more well-fitting spin state solutions within the modeling uncertainty (i.e. detailed satellite geometry, reflective properties). Also, there is strong evidence that the YORP effect drives satellites from uniform rotation to non-principal axis tumbling. Such tumbling states further complicate the light curve inversion process because tumbling motion is driven by two independent periods. To aid spin state analysis, particularly for the tumbling case, we incorporate Doppler radar observations obtained at the Goldstone Deep Space Communications Complex. Studying the family of well-known retired GOES weather satellites, we obtain unambiguous spin period estimates for all targets and greatly narrow pole solutions, independent of light curve data. We note significant changes in spin rates and pole directions over a two month span. These findings are consistent with YORP-driven evolution.

1. INTRODUCTION

The debris population near geosynchronous earth orbit (GEO) continues to grow with ongoing launches and no natural deorbit mechanisms. Understanding the long-term dynamical evolution of these debris objects is necessary to protect active assets and preserve GEO for future use. In spite of this, research on the long-term spin state evolution of GEO debris has been limited. The spin states of GEO debris, particularly retired and otherwise defunct satellites, are known to be diverse and evolve significantly over time [1-7]. A better understanding of long-term defunct satellite spin state evolution would aid GEO space situational awareness, prediction of attitude-dependent debris perturbations (e.g. solar radiation pressure), active debris removal, satellite servicing, anomaly resolution, and also provide insight about small asteroid rotational evolution. Recent observations and dynamical simulations have shown that the spin states of some defunct GEO satellites are predominantly driven by the Yarkovsky-O'Keefe-Radzievskii-Paddack (YORP) effect [5-9]. The YORP effect is spin state evolution caused by solar radiation and thermal re-emission torques [10].

Observations are valuable to gain direct insight and validate theories about defunct GEO satellite spin state evolution. Unfortunately, extracting GEO satellite spin states (i.e. spin periods and attitude) from ubiquitous photometric light curve observations can be challenging, even for known satellites. Fitting satellite spin states often results in numerous local minima, even with high fidelity (e.g. ray-traced) photometric models. A number of defunct GEO satellites are also in non-principal axis rotation (i.e. tumbling), and recent work indicates that the YORP effect can cause defunct satellites to transition from uniform rotation to tumbling where their dynamical evolution continues [5-9]. Tumbling light curve analysis is more challenging than the uniform rotation case because there are two fundamental spin periods: $P_{\bar{\phi}}$ corresponding to precession of the satellite's long axis around the rotational

angular momentum vector $\vec{H}$ (pole) and P_ψ to rotation of the long axis about itself [5]. These periods are illustrated in Figure 1 for the GOES 8 satellite. Dominant light curve frequencies for tumblers consist of several or more (*a priori* unknown) low-order harmonics of the two fundamental frequencies [5]. The common analysis approach requires testing candidate tumbling period pairs over the sphere of possible attitude phasing and angular momentum vector directions [5], often resulting in a number of similarly well-fitting period pairs and complete solutions.

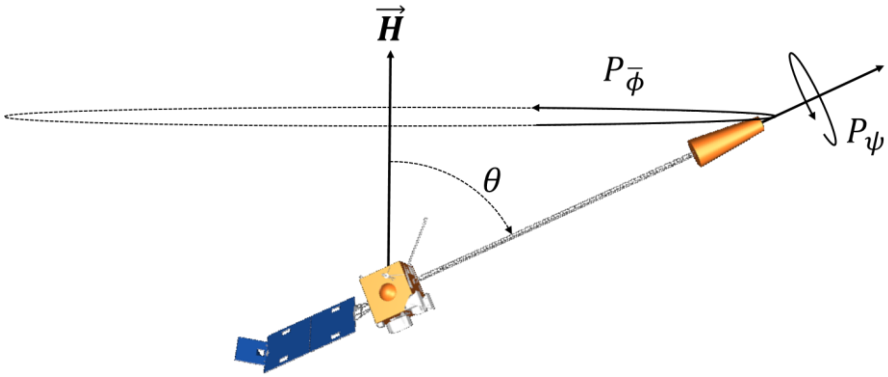

Fig. 1: Long Axis Convention Tumbling Periods for GOES Satellite

The aim of this work is to reduce light curve spin state ambiguity by incorporating Doppler radar measurements obtained using the 34 m antennas at NASA's Goldstone Deep Space Communications Complex in California. Unlike, non-resolved photometric light curves, Doppler radar provides spatial resolution of a spinning target. This allows for unambiguous identification of the long axis precession (i.e. spin period) for both uniform rotators and tumblers. Furthermore, Doppler provides pole information that is much easier to interpret and a potentially unambiguous pole solution given advantageous geometry. Overall, radar and optical data are complementary. Optical provides rich period harmonics and detailed attitude information, while radar provides the precession period and greatly constrains the pole. Final detailed fitting of the optical data can potentially yield an unambiguous complete spin state solution.

In the remainder of the paper, we first outline our simple radar model and spin state estimation techniques. We then discuss our experiment setup, including the target GOES 8-12 satellites. These retired NOAA weather satellites have significant asymmetry making them highly susceptible to the YORP effect and facilitating radar echo interpretation. Their geometry and mass properties are well-documented, further aiding echo analysis [10]. We then present and analyze the resulting observations, discuss our findings, and finally provide conclusions.

2. APPROACH

2.1 Simple Radar Model

We will start by discussing the Doppler observables and our simulated radar model used to test the spin state estimation techniques. The observed Doppler shift f_d is given by the following equation,

$$f_d = -2\dot{R}/\lambda_t \tag{1}$$

where λ_t is the transmitted radar wavelength, and $\dot{R}$ is the range-rate between the ground-based antenna and a fixed location on the target.

To calculate simulated Doppler echoes, the vector $\vec{R}_i$ from the ith satellite facet to radar antenna is given by,

$$\vec{R}_i = \vec{s} - \vec{r}_i \tag{2}$$

where $\vec{r}_i$ is the position vector from the satellite center of mass to the facet centroid, and $\vec{s} = s\hat{s}$ is the vector from the satellite center of mass to the radar antenna (calculated using JPL NAIF SPICE ephemerides and TLEs). Then, assuming $\vec{r}_i \ll \vec{s}$, the facet's range-rate $\dot{R}_i$ due solely to satellite rotation is given by,

$$\dot{R}_i = -\left[\left(\vec{\omega} - \vec{\omega}_{S/N}\right) \times \vec{r}_i\right] \cdot \hat{s} \tag{3}$$

where $\vec{\omega}$ is the satellite's inertial angular velocity and $\vec{\omega}_{S/N} = -\frac{1}{s}\dot{\hat{s}} \times \hat{s}$ is the inertial rate of change of $\hat{s}$ (roughly 15°/hr for GEO satellites). The spacecraft attitude and $\vec{\omega}$ are obtained by numerically integrating the satellite's torque-free rotation. The echo power of each facet P_i is simply given by,

$$P_i = \rho_i A_i \max(\hat{s} \cdot \hat{n}_i, 0)^2 \tag{4}$$

where ρ_i is the facet radar reflectivity, A_i is its area, and $\hat{n}_i$ is its outward unit normal vector. The max() function ensures that facets only provide echoes when $\hat{s}$ is above the facet horizon. To obtain Doppler vs. time plots, the facet power is then binned by its corresponding Doppler frequency.

Figure 2 shows the shape model of the defunct GOES 8 satellite in the principal axis frame consisting of roughly 1000 facets. The large number of facets helps fill the Doppler spectrum. The GOES satellites are highly asymmetric with a single solar panel and long conical solar sail to balance solar torques during earth-pointing operation.

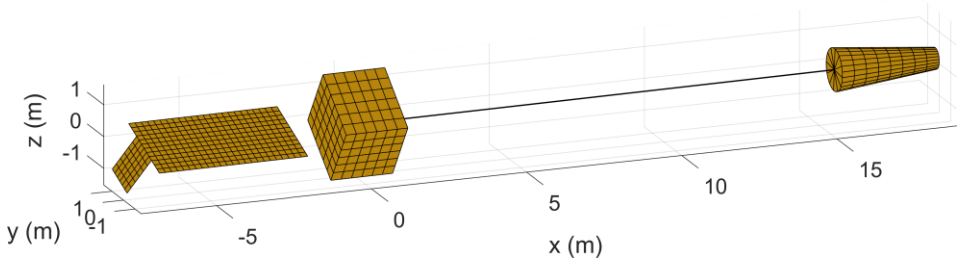

Fig. 2: GOES 8 Shape Model

Simulating Doppler echoes, the satellite model is placed in uniform rotation about the maximum inertia (z) axis with $P_{\bar{\phi}} = 216$ s. The radar reflectivity of all facets is set equal. Figure 3 shows simulated Doppler echoes vs. time with brighter echoes denoting higher echo power. The sinusoidal +/-15 Hz echoes correspond to the conical solar sail as this is farthest from the satellite center of mass and therefore has the largest radial velocity. The +/-5 Hz solar panel echoes are directly out of phase with the sail echoes since these parts are on opposite sides of the satellite. The ~216 s periodicity is clearly evident from the sail and solar panel echoes. This observed period $P_{\bar{\phi}}^{syn}$ will differ slightly from the true period $P_{\bar{\phi}}$ due to non-zero $\vec{\omega}_{S/N}$. Finally, around +/-1 Hz we see the bright bus echoes. With significant implications for pole estimation, we see a notable increase in Doppler bandwidth over time. With the satellite's pole inertially fixed, the projection of the satellite's rotational velocity along the time-varying $\hat{s}$ changes, resulting in increasing Doppler bandwidth over time.

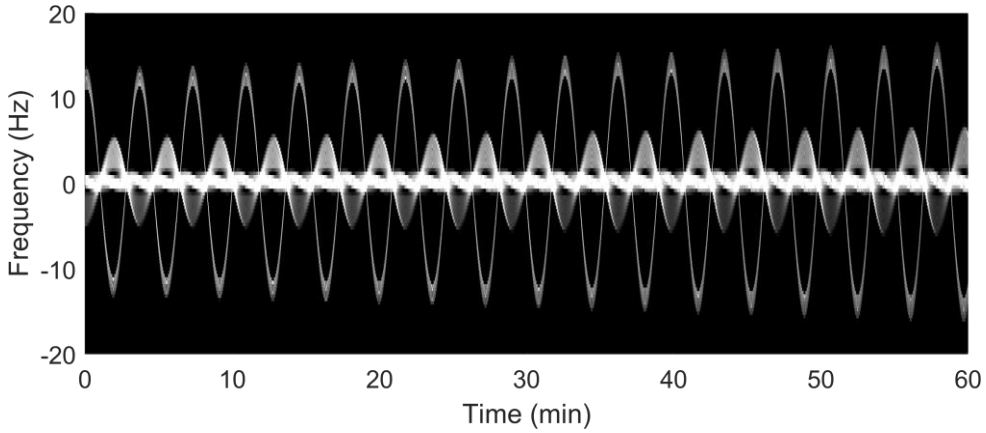

Fig. 3: Simulated GOES 8 Doppler Echoes ($P_{\bar{\phi}} = 216$ s)

2.2 Doppler Bandwidth Pole Estimation

We will now discuss the spin pole estimation techniques used in this paper, starting with the simplest, Doppler bandwidth. This method requires knowledge of the satellite's maximum radial extent from the center of mass (known for the GOES satellites). First, with r denoting the satellite's maximum radial extent and α the angle between $\hat{H}$ and $\hat{s}$ (see Fig. 4), the maximum range-rate of a facet (assuming uniform rotation with $\vec{\omega}_{S/N} \ll \vec{\omega}$) is,

$$\dot{R}_{max} = \frac{2\pi r \sin\alpha}{P_{\bar{\phi}}} \tag{5}$$

With Eq. 1, we can solve for α in terms of the observed maximum Doppler bandwidth b,

$$\sin\alpha = \frac{\lambda_t P_{\bar{\phi}} b}{4\pi r} \tag{6}$$

For Doppler bandwidth, we assume $P_{\bar{\phi}} = P_{\bar{\phi}}^{syn}$ (a good approximation if $\vec{\omega}_{S/N} \ll \vec{\omega}$). To estimate $P_{\bar{\phi}}^{syn}$ from radar, we simply phase fold the Doppler echoes. With this method, the time steps are binned by rotational phase. With a bin for each Doppler frequency and rotational phase pair, the dispersion in echo power over successive rotations is calculated. Sweeping over candidate periods, the period minimizing overall dispersion is selected.

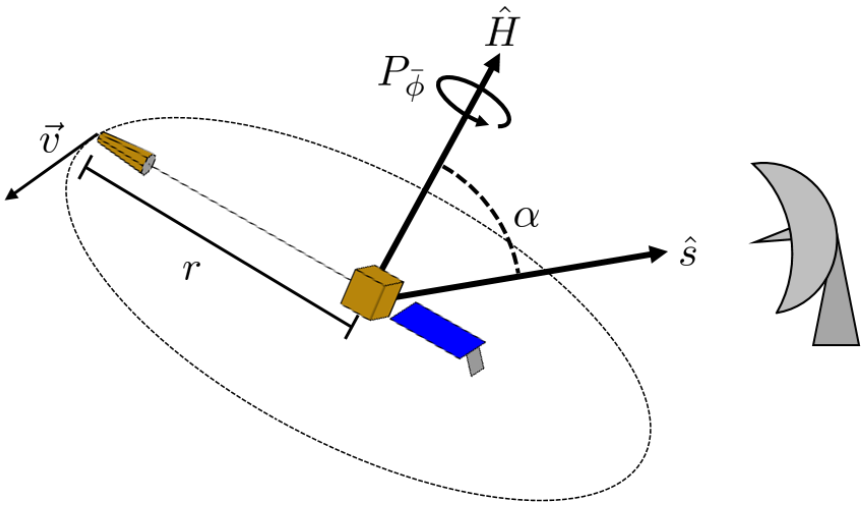

Fig. 4: Doppler Bandwidth Illustration

At a given epoch, Eq. 6 yields two cones on which $\hat{H}$ lies (only one if $\sin\alpha = 1$). Echoes obtained from significantly different $\hat{s}$ directions yield additional cones. Assuming the pole is inertially fixed, viable pole solutions must lie on the intersection of cones from all epochs. With a single or two closely spaced transmitting/receiving antennas, the well-spaced $\hat{s}$ directions can be obtained by observing the GEO target every several hours or at different local times on subsequent days.

Sample GOES 8 Doppler bandwidth analysis is provided in Figure 5. The simulated Doppler echoes are provided in the top plot. The dashed white line denotes the maximum possible bandwidth for the given $P_{\bar{\phi}}$ (216 s). The colored time stamps denote the observation times. Proceeding from t_1 to t_3, b decreases from ~23 Hz to ~15 Hz. Solving Eq. 6 and plotting the resulting cones, we obtain four candidate poles shown in the bottom plot of Figure 5. Note that the upper left solution with R.A. = 90° and declination = 45° is the correct one. In general, Doppler bandwidth yields at least two pole solutions.

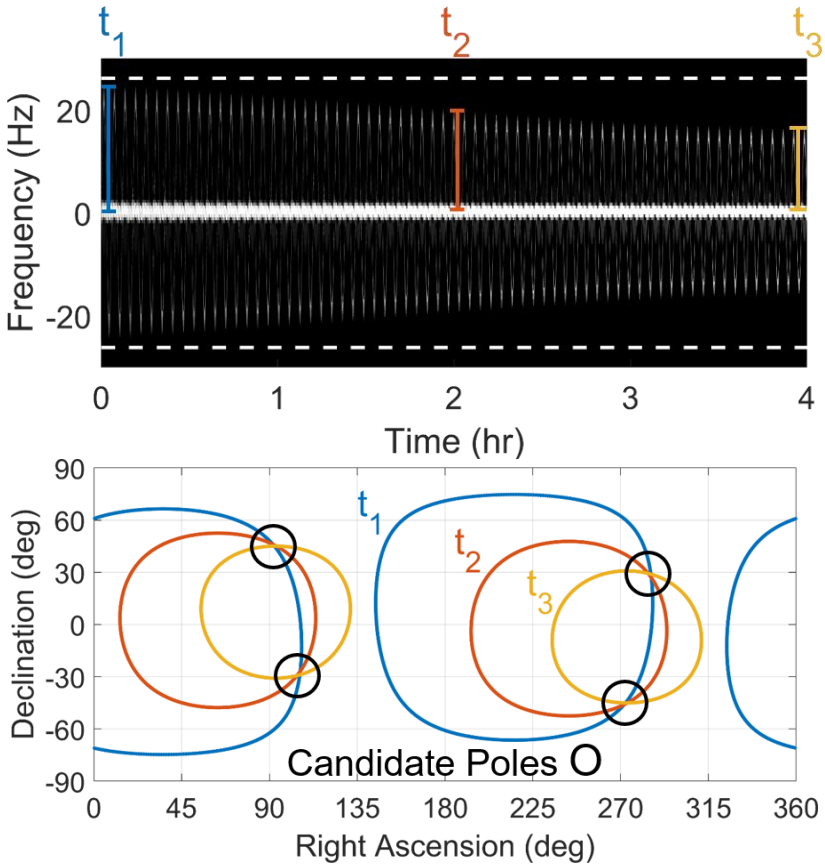

Fig. 5: (*top*) Simulated Doppler echoes and (*bottom*) candidate pole directions (true solution is R.A. = 90° and declination = 45°)

2.3 3D Rotationally Phased Doppler (RPD) Pole Estimation

While straightforward, the Doppler bandwidth approach yields at least two candidate pole solutions and requires knowledge about the satellite's maximum radial extent. To hopefully overcome these limitations, we explore another technique. With three or more receiving antennas in a well-spaced, non-planar configuration, one can directly solve for an object's instantaneous velocity. Assuming $\vec{r}_i \ll \vec{s}$ and $\vec{\omega}_{S/N} \ll \vec{\omega}$, both strong assumptions for GEO satellites, Eq. 1 can be written in matrix form for three (or more) receiving antennas denoted 1, 2, and 3

$$\begin{bmatrix} f_{d_1} \\ f_{d_2} \\ f_{d_3} \end{bmatrix} = -\frac{2}{\lambda_t} \begin{bmatrix} \hat{s}_1^T \\ \hat{s}_2^T \\ \hat{s}_3^T \end{bmatrix} \vec{v}(\tau) \tag{7}$$

where $\vec{v}(\tau)$ is the inertial rotational velocity of a part of the satellite at time τ and $\hat{s}_1$, $\hat{s}_2$, and $\hat{s}_3$ denote the 3×1 unit vectors from the satellite to each receiving antenna (see Figure 6). With $\hat{s}_1$, $\hat{s}_2$, and $\hat{s}_3$ well-spaced and non-planar, we can invert Eq. 7 to solve directly for $\vec{v}(\tau)$.

Unfortunately for GEO observation, the receiving antennas must be in a triangular configuration 1000s of km apart. In most practical applications, obtaining and coordinating three or more large antennas separated by these distances is not possible. For example, at NASA Goldstone, the antennas are separated by no more than 20 km (angular separation at GEO of ~0.03°). This is not sufficient for the above inversion.

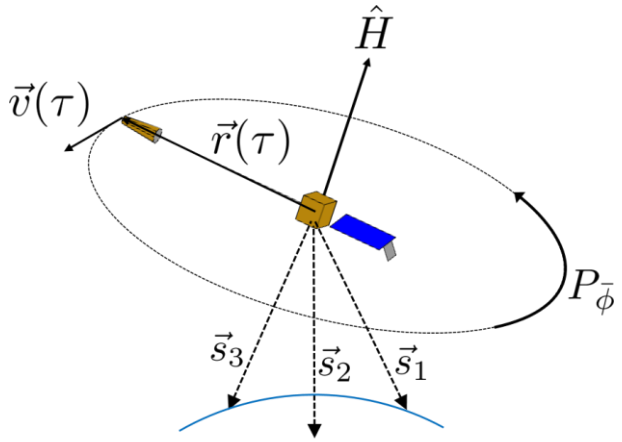

Fig. 6: Rotationally Phased Doppler Illustration

To overcome this practical limitation in the case of a single transmitting/receiving antenna, we leverage the periodicity of the satellite's rotation. Assuming the satellite is in uniform rotation with a fixed spin rate and pole direction, the inertial position $\vec{r}(\tau)$ and velocity $\vec{v}(\tau)$ vectors of a part of the satellite with respect to the center of mass (e.g. GOES 8's solar sail in Figure 6) are periodic in $P_{\bar{\phi}}$. In other words,

$$\begin{aligned} \vec{r}\left(\tau + nP_{\bar{\phi}}\right) &= \vec{r}(\tau) \\ \vec{v}\left(\tau + nP_{\bar{\phi}}\right) &= \vec{v}(\tau) \end{aligned} \tag{8}$$

where n is an integer. So now, instead of $\hat{s}_1$, $\hat{s}_2$, and $\hat{s}_3$ being the directions to each of three antennas at the same time, they are the directions from the satellite to a single receiving antenna at three different times spaced by multiples of $P_{\bar{\phi}}$,

$$\begin{aligned} \hat{s}_1(\tau) &= \hat{s}\left(\tau + n_1 P_{\bar{\phi}}\right) \\ \hat{s}_2(\tau) &= \hat{s}\left(\tau + n_2 P_{\bar{\phi}}\right) \\ \hat{s}_3(\tau) &= \hat{s}\left(\tau + n_3 P_{\bar{\phi}}\right) \end{aligned} \tag{9}$$

Observations in phase with the satellite's rotation are used so that the "same" velocity vector is observed at each time. Provided the observer lines of sight are sufficiently well-spaced and non-planar as the satellite orbits, one can directly solve for $\vec{v}(\tau)$ using Eq. 7. Repeating this analysis for successive rotational phases (i.e. slightly later starting times τ), one can trace out the $\vec{v}(\tau)$ rotational plane and therefore the pole direction $\hat{H}$ with the right hand rule.

There is a complication for this rotationally phased Doppler (RPD) approach, namely estimation of $P_{\bar{\phi}}$. Solutions for $\vec{v}(\tau)$ with be very sensitive to the estimated value for $P_{\bar{\phi}}$, as illustrated in the lower plot of Figure 8. As noted above, the observed period $P_{\bar{\phi}}^{syn}$ will likely differ slightly from the true inertial value $P_{\bar{\phi}}$. We know that for uniform rotation with a fixed spin rate, the velocity magnitude $|\vec{v}(\tau)|$ is constant. So with the above echo phase-folding technique we obtain $P_{\bar{\phi}}^{syn}$. From there, we sweep over candidate $P_{\bar{\phi}}$'s around $P_{\bar{\phi}}^{syn}$, obtaining solutions for $\vec{v}(\tau)$ for many rotational phases (preferably one full satellite rotation). We then find the candidate $P_{\bar{\phi}}$ that yields the smallest dispersion in $|\vec{v}(\tau)|$ over one satellite rotation. This $P_{\bar{\phi}}$ estimate can then be used to obtain our pole solution.

To illustrate this RPD approach, we will now provide simulated analysis. We use the GOES 8 model and place it in the 14.9° inclination orbit of defunct GEO satellite Telstar 401 on April 30, 2020. Assuming an arbitrary and precise $P_{\bar{\phi}} = 216.4493$ s and pole right ascension and declination of 0° and 45° respectively, Doppler spectra are recorded at a 2 s cadence over the course of 8 hr assuming a single antenna located in Goldstone, California. Phase-folding the initial 30 min of data, we obtain a minimum dispersion $P_{\bar{\phi}}^{syn}$ = 217 s.

Analyzing observations at the beginning, middle, and end of this 8 hr arc (see Figure 7), we manually fit local sinusoids to the outermost (i.e. solar sail) Doppler echoes. These sinusoids are shown as red lines in Figure 7. Continuous local fits are useful since we sweep over candidate $P_{\bar{\phi}}$ values and sample the Doppler at different times.

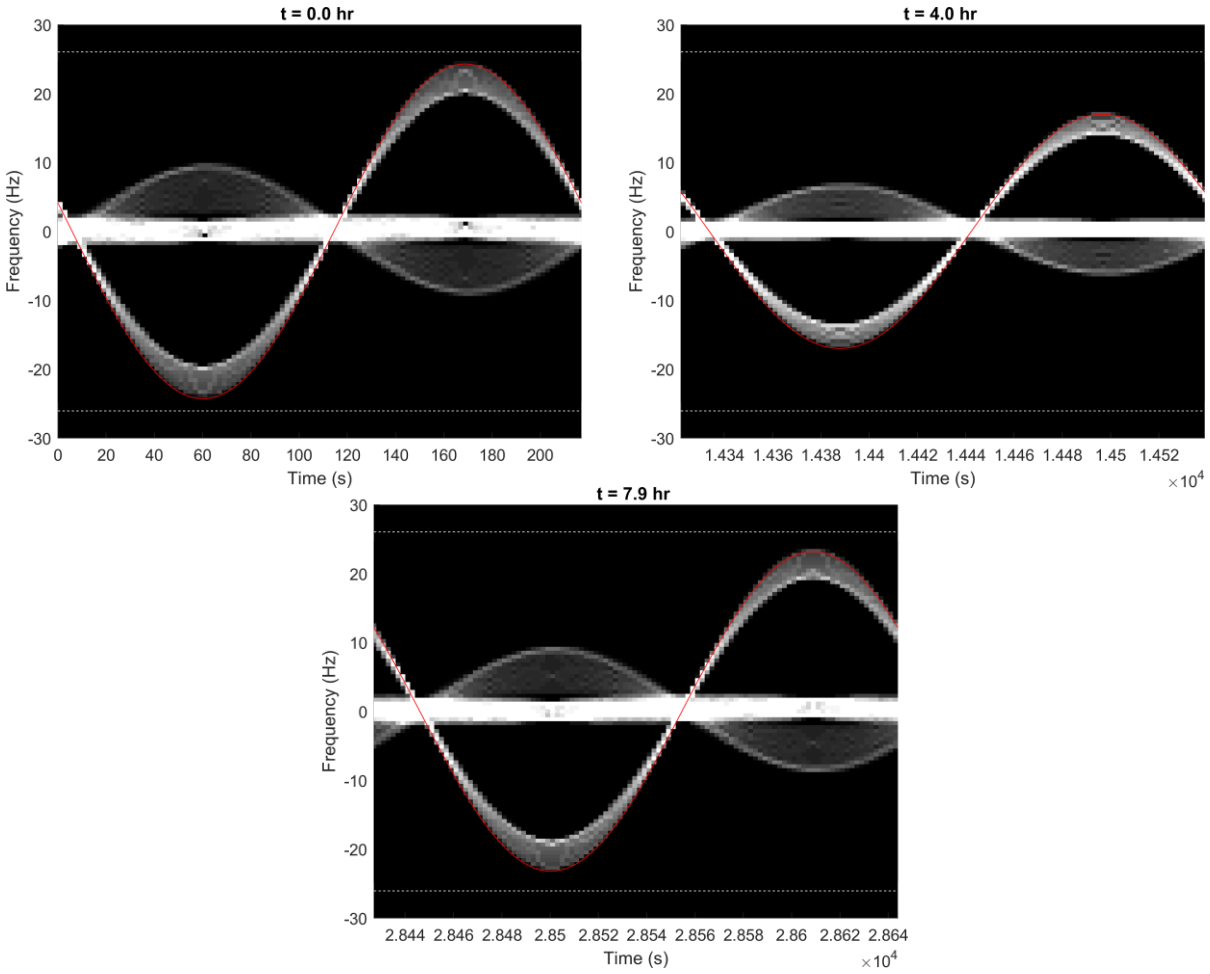

Fig. 7: Doppler echoes at multiples of $P_{\bar{\phi}}^{syn}$. The red lines are locally fit sinusoids to the solar sail Doppler.

Solving for $\vec{v}(\tau)$ at 22.5° increments of rotational phase from 0° to 360° using the locally fit sinusoids from Figure 7, the resulting velocity magnitude standard deviation for candidate $P_{\bar{\phi}}$'s are provided in the top plot of Figure 8. Note that the $P_{\bar{\phi}}$ resolution was 0.001 s. Here, we see a sharp dip in dispersion at 216.450 s where the standard deviation in $|\vec{v}|$ over these 22.5° increments is 1.5 mm/s (0.3% of the nominal $|\vec{v}|$). Taking this as our $P_{\bar{\phi}}$ estimate, the bottom plot in Figure 8 provides the pole estimate. From Figure 8, we can see that the pole estimate is very sensitive to the assumed $P_{\bar{\phi}}$ value. The resulting spin state estimates are provided in Table 1 along with the prescribed truth values. Since the GOES satellite has a known radial extent (18.87 m from center of mass to the end of the solar sail), this can also be compared to the derived extent $|\vec{v}|_{mean} P_{\bar{\phi}}/2\pi$. All parameters agree very well for our simulated case.

Table 1: Simulated Rotationally Phased Doppler (RPD) Pole Estimation Results

	$P_{\bar{\phi}}$	Right Ascension	Declination	Radial Extent
Truth	216.4493 s	0°	45°	18.87 m
Estimate	216.450 s	-0.4°	44.75°	18.997 m

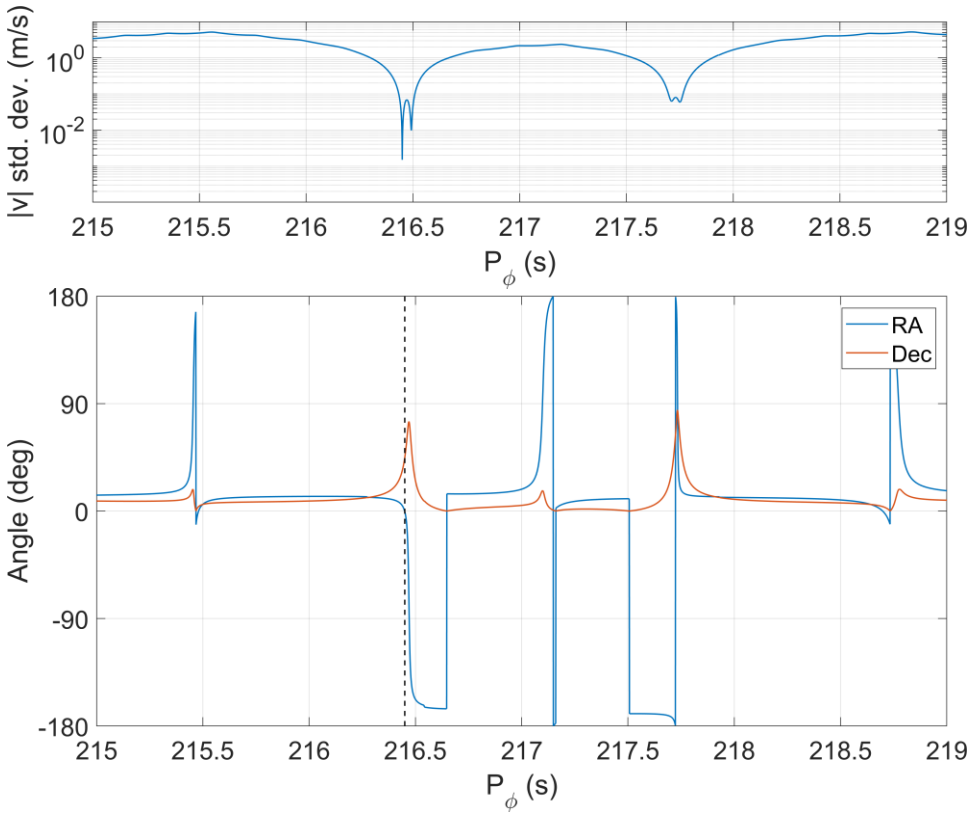

Fig. 8: (*top*) $|\vec{v}|$ standard deviation over rotational phase vs. candidate $P_{\bar{\phi}}$, (*bottom*) Pole right ascension and declination vs. candidate $P_{\bar{\phi}}$ with the dashed line denoting the minimum dispersion $P_{\bar{\phi}}$ value (216.450 s)

Summarizing this RPD pole estimation approach, with sufficiently well-spaced and non-planar observation directions, a precise long axis precession period estimate $P_{\bar{\phi}}$ can be obtained along with an unambiguous pole estimate using Doppler echoes from a single transmitting/receiving antenna. Importantly, we assume that the satellite's pole and spin rate are fixed. This approach does not require detailed knowledge of an object's geometry or reflective properties, only the presence of distinguishing features far from the center of mass that can be identified over successive rotations (e.g. solar sail, solar array outer edge, upper stage rocket nozzle). For GEO objects, high inclinations are advantageous as they provide the necessary non-planar observation geometry. Once $P_{\bar{\phi}}^{syn}$ is obtained, observing tracks are only needed every several hours covering 1-2 rotation periods each. So the antenna operators can cycle between several targets over one observing session. For MEO and GTO objects, the smaller semi-major axes and often large inclinations allow for shorter observation arcs to yield the same line of sight variation with only marginal increase in $\vec{\omega}_{S/N}$. Shorter arcs are useful as the satellite's spin state could be slowly changing due to environmental torques.

2.4 2D Rotationally Phased Doppler (RPD) Pole Estimation

For shorter observing sessions and/or low inclination satellites, this 3D RPD approach can be reduced to two dimensions for known satellites, yielding two candidate pole solutions (because the sign of the out of plane velocity component is unconstrained). Denoting $\beta_i(\tau)$ as the angle between the instantaneous velocity $\vec{v}(\tau)$ and the observer direction $\hat{s}_i(\tau)$ we have,

$$\cos\beta_i(\tau) = -\frac{\lambda_t P_{\bar{\phi}} f_{d_i}(\tau)}{4\pi r} \tag{10}$$

Eq. 10 yields a single cone around $\hat{s}_i(\tau)$ on which $\vec{v}(\tau)$ lies. Using three or more observations spaced at multiples of the candidate $P_{\bar{\phi}}$, we find the value of $P_{\bar{\phi}}$ where all cones intersect at the same two points (i.e. self-consistent

inertial velocity direction) . This provides the two possible solutions for the velocity direction at that rotational phase. Solving at successive rotational phases yields additional velocities, providing the two candidate rotation planes and pole directions.

3. EXPERIMENT

With the aim of obtaining spin rate and pole estimates for defunct GEO satellites, our experiment targets consisted of four retired GOES weather satellites: GOES 8, GOES 10, GOES 11, and GOES 12. These satellites have been studied extensively with optical observations showing diverse spin states with significant spin period variation over time, with strong indication of YORP-driven behavior [2,3,5-7]. For example, starting with a spin period of 16.83 s in late 2013, GOES 8 spun down rapidly through 2014 and transitioned to non-principal axis tumbling with a long axis precession period >20 min [2,3,5,6]. It has since began spinning back up with photometry indicating a 4.88 min precession period by April 2018 [5]. These satellites are therefore dynamically interesting. Also, their significant asymmetry and known geometry and mass properties greatly aid Doppler echo analysis [11]. Overall, these attributes make these satellites ideal targets for radar study.

Subsets of these GOES satellites were observed from Goldstone on December 6, 2019 and February 18-20, 2020. Avoiding radar illumination of all other catalogued spacecraft, two 34 meter Deep Space Network (DSN) antennas were used in a bi-static configuration with one antenna transmitting and the second receiving the reflected echoes. The transmitted signal consisted of fixed frequency, continuous wave carrier at X-band. We alternated periodically between several targets over the course of the night to sample different inertial viewing directions for each one. On several nights, near-simultaneous photometry was collected at Magdalena Ridge Observatory (MRO) in New Mexico.

With the echoes recorded, windowed FFT analysis was conducted to obtain Doppler spectra vs. time. Adjustment of the FFT integration time allowed for tradeoff between temporal and frequency resolution. To maintain roughly equal bandwidth and rotational phase bins for all observations, FFT integration times were adjusted for the observed precession periods. With a fixed frequency carrier, orbital Doppler was removed in post-processing using TLEs for the satellites and JPL NAIF SPICE ephemerides for the antennas.

4. RESULTS

4.1 GOES 8

Doppler echoes for GOES collected on December 6, 2019 are provided in Figure 9. Comparing with Figure 1, we can clearly identify the solar sail, solar panel, and bus echoes. Phase-folding the observations yielded $P_{\dot{\phi}}^{syn}$ = 353 s (5.9 min). There are additional rotating features visible that lag roughly 45° behind the solar sail sinusoid (e.g. at +4 Hz at ~700 s and ~1100 s in the top plot and 400s and 2500 s in the bottom plot). These are likely due to the satellite's magnetometer boom and/or telemetry and control antenna which protrude several meters from the bus (see Figure 1). Tracing these features through both plots, we see that their amplitude varies over successive precession periods, indicating long axis rotation and therefore non-principal axis tumbling. With long axis rotation, the projected area of the solar array along $\hat{s}$ would change, likely affecting the echo power. This is consistent with the varying solar panel echo power over successive rotations, most notably in the top plot of Figure 8. Also, we see that the observed Doppler bandwidth in the top plot is nearly equal to the maximum expected bandwidth for the observed spin period, indicating we are viewing the pole roughly side-on. Moving to the bottom plot, we see a notable decrease in Doppler bandwidth indicating a more pole-on view.

We analyzed the Dec. 6, 2019 GOES 8 echoes with the Doppler bandwidth and 2D RPD techniques to obtain candidate poles. The relatively short arc and resulting near-planar observing geometry made the 3D RPD approach infeasible. $\dot{\phi}$ is almost constant for the tumbling GOES satellites since they are nearly axisymmetric. So GOES 8's motion was assumed to be uniform, allowing us to use the Doppler bandwidth and 2D RPD approaches. The resulting solutions are provided in Figure 10 in the J2000 ecliptic frame to allow for natural comparison with the sun and anti-sun directions (shown as filled and open circles respectively). The Doppler bandwidth approach yields eight possible pole solutions (in four compact regions). 2D RPD eliminates two of these regions. Overall, this analysis suggests GOES 8's pole is below the ecliptic plane with ecliptic longitude $\lambda \sim 150°$ and ecliptic latitude $\delta \sim$ -30° or $\lambda \sim 300°$ and $\delta \sim$ -23°.

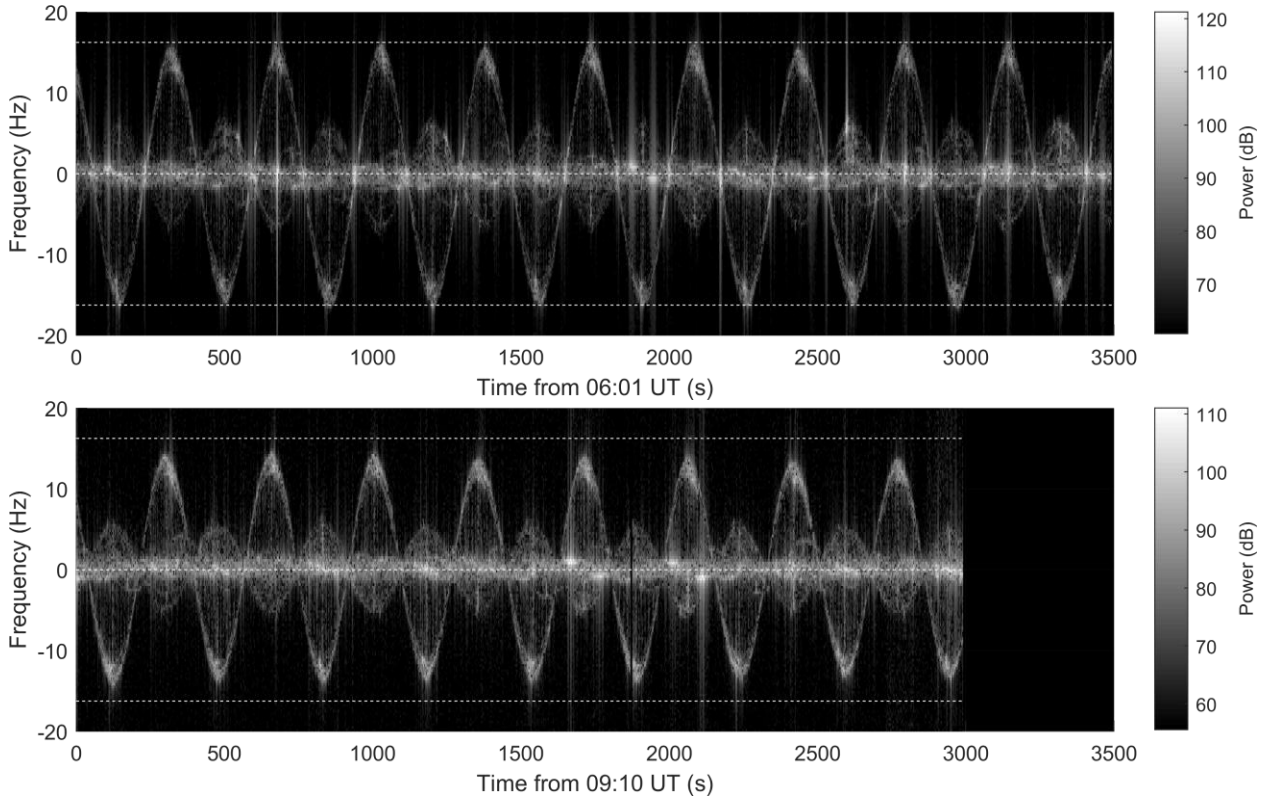

Fig. 9: Dec. 6, 2019 GOES 8 echoes. The outer dashed lines denote the maximum expected bandwidth for the observed precession period $P_{\dot{\phi}}^{syn} = 353$ s (5.9 min).

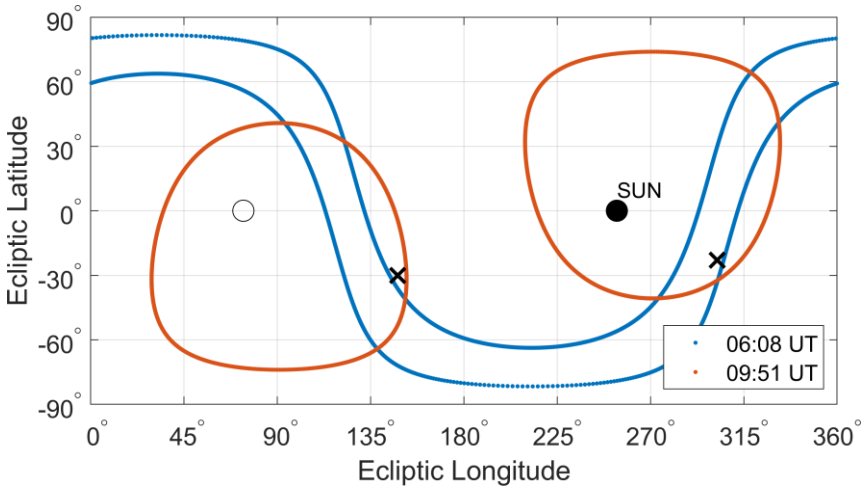

Fig. 10: Dec. 6, 2019 GOES 8 Candidate Poles in the J2000 Ecliptic Frame. The colored lines represent the Doppler Bandwidth solutions. The two crosses mark the 2D Rotationally Phased Doppler solutions. The open circle is the anti-sun direction.

Continuing out in time, Figure 11 shows GOES 8 Doppler echoes obtained on February 18, 2020. Phase-folding the Feb. 18 observations yielded $P_{\dot{\phi}}^{syn}$ = 216 s (3.60 min). Compared to Figure 9, the increase in spin rate is immediately apparent. This increased spin rate is accompanied by larger Doppler bandwidth given the larger maximum solar sail radial velocity. On February 18, GOES 8 photometry was also obtained at Magdalena Ridge Observatory. The reduced light curve is provided in the left plot of Figure 12. From previous study of the GOES satellites [5], the complexity of this light curve is clear indication of non-principal axis tumbling. With $P_{\dot{\phi}}^{syn}$ unambiguously provided

by radar, we would like to estimate the long axis rotation period P_ψ. Fitting the light curve with a fourth order (m = 4) two dimensional Fourier series [12] across a range of candidate P_ψ values, we obtain the best-fitting solution with P_ψ = 17.94 min. Interestingly, this is almost exactly 5 times $P_{\bar{\phi}}^{syn}$. Again, the light curve is much too complex for uniform rotation. Furthermore, Lomb-Scargle periodogram analysis (used instead of FFT analysis due to observation gaps) showed significant frequencies at 0.057, 0.34, 0.39, and 0.56 min^{-1}. These correspond to f_ψ, $f_{\bar{\phi}} + f_\psi$, $f_{\bar{\phi}} + 2f_\psi$, and $2f_{\bar{\phi}}$, with $2f_{\bar{\phi}}$ having the highest significance by a factor of two. These are common harmonics for tumbling GOES satellites [5]. Phase-folding the light curve (right plot of Figure 12), we find that it repeats almost exactly on this candidate P_ψ. Since GOES 8 is nearly axisymmetric, if the two fundamental tumbling periods $\overline{P_\phi}$ and P_ψ are multiples of each other, the satellite will periodically return to the same inertial attitude and have a nearly periodic light curve. Closely inspecting Figure 11, the magnetometer/antenna echoes repeat after five precession periods, suggesting the satellite has returned to the same inertial attitude. The first appearance is at 260 s and +5 Hz and they return to the same spot relative to the solar sail echoes at 1340 s and +5 Hz. Overall, these findings strongly indicate the satellite is in a 5:1 tumbling resonance with tumbling periods $P_{\bar{\phi}} \sim$ 3.60 min and $P_\psi \sim$ 17.94 min.

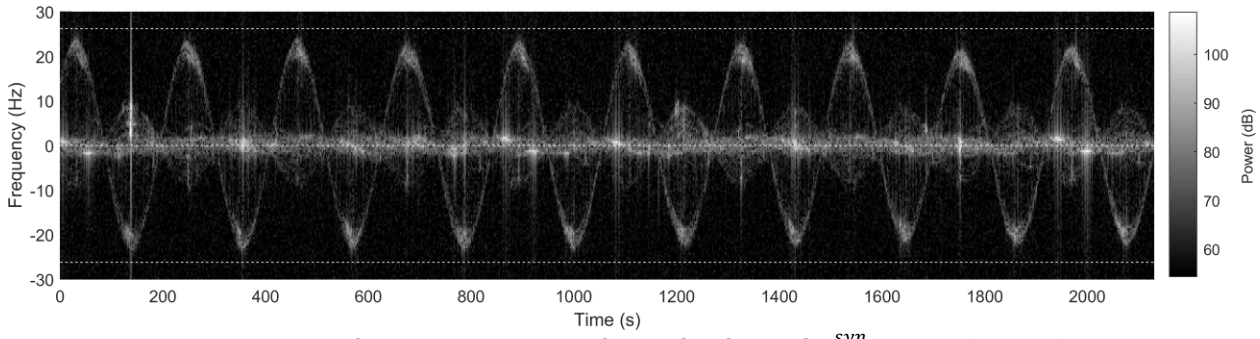

Fig. 11: Feb. 18, 2020 GOES 8 echoes. The observed $P_{\bar{\phi}}^{syn} = 216$ s (3.6 min).

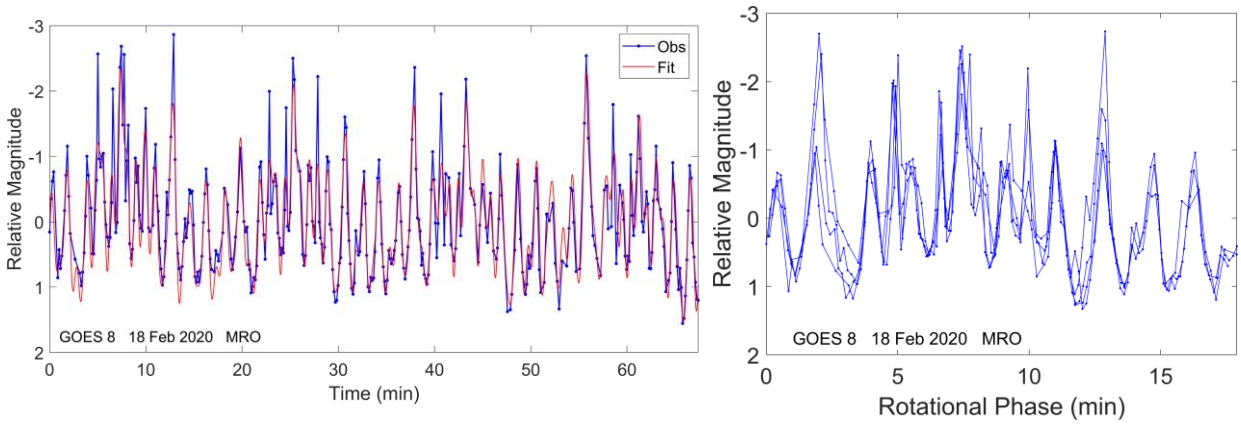

Fig. 12: Feb. 18, 2020 GOES 8 Light Curve (*left*) with 2D Fourier Series Fit (m=4) with $P_{\bar{\phi}}$ = 3.60 min, P_ψ = 17.94 min [12], (*right*) Light Curve Phase-Folded on P = 17.92 min

Figure 13 shows the candidate poles for GOES 8 on February 18, 2020. We see that the Doppler bandwidth solutions and 2D RPD solutions are quite consistent with one another indicating the pole has $\lambda \sim 135°$ and $\delta \sim 15°$ or $\lambda \sim 325°$ and $\delta \sim 25°$. Fortunately, the GOES 8 observation geometry was well-enough spaced on this day to attempt 3D RPD analysis. The tentative 3D RPD solution is shown as a black diamond in Figure 13 and is close to the left-most Doppler bandwidth/2D RPD solution. We are somewhat confident in this 3D RPD solution because it yielded almost exactly the same $P_{\bar{\phi}}$ estimate as the 2D RPD solution (~215.0 s) with a derived radial extent of ~22 m (only 17% more than GOES 8's known boom length). Regardless, both candidate solutions place GOES 8's pole within 30° of the sun/anti-sun line. Furthermore, the two pole solutions obtained from Feb. 20, 2020 GOES 8 Doppler echoes were virtually the same as for February 18, increasing our confidence in these candidate solutions.

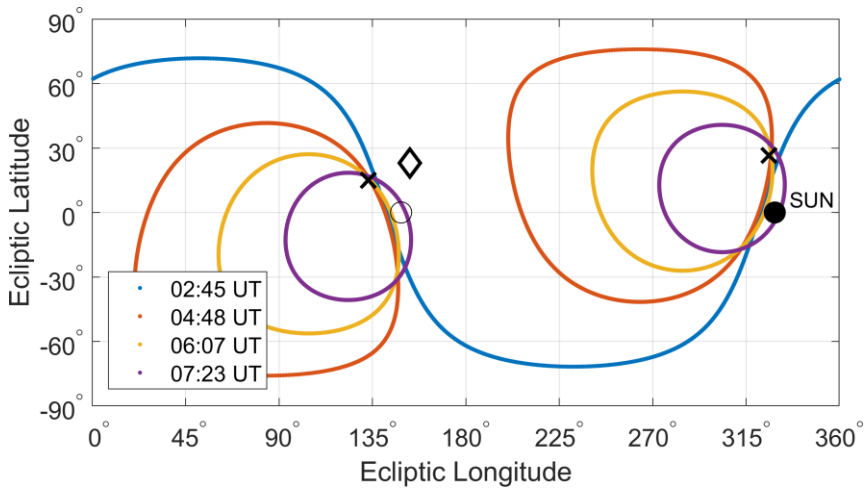

Fig. 13: Feb. 18, 2020 GOES 8 Candidate Poles. The black diamond denotes the tentative 3D RPD solution.

4.2 GOES 10

GOES 10 Doppler echoes on Feb. 18, 2020 are provided in Figure 14. We see rapid rotation with $P_{\bar{\phi}} \approx 30.5$ s and Doppler exceeding +/- 150 Hz. Utilizing all observations which spanned roughly three hours, the four Doppler bandwidth candidate pole estimates are provided in Figure 15 along with the two possible solutions provided by 2D RPD. These 2D RPD solutions are near two Doppler bandwidth solutions, differing slightly in longitude. The Doppler bandwidth solutions indicate the pole has either $\lambda \sim 45°$ and $\delta \sim 40°$ or $\lambda \sim 180°$ and $\delta \sim 67°$.

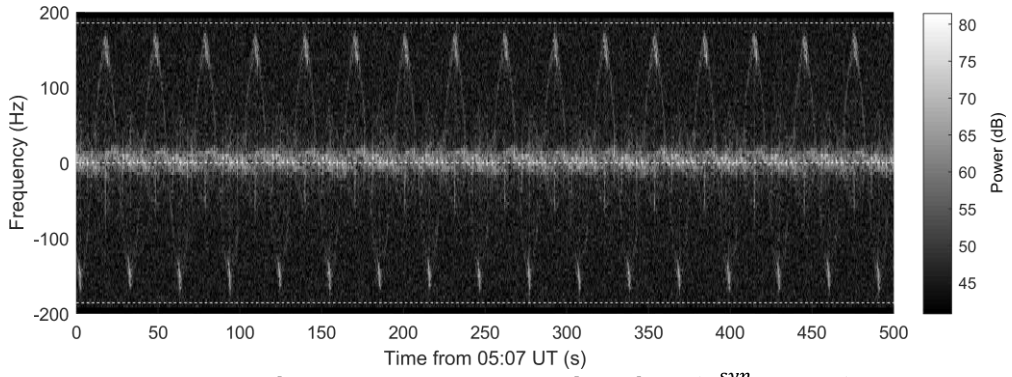

Fig. 14: Feb. 18, 2020 GOES 10 Doppler Echoes ($P_{\bar{\phi}}^{syn}$ = 30.5 s)

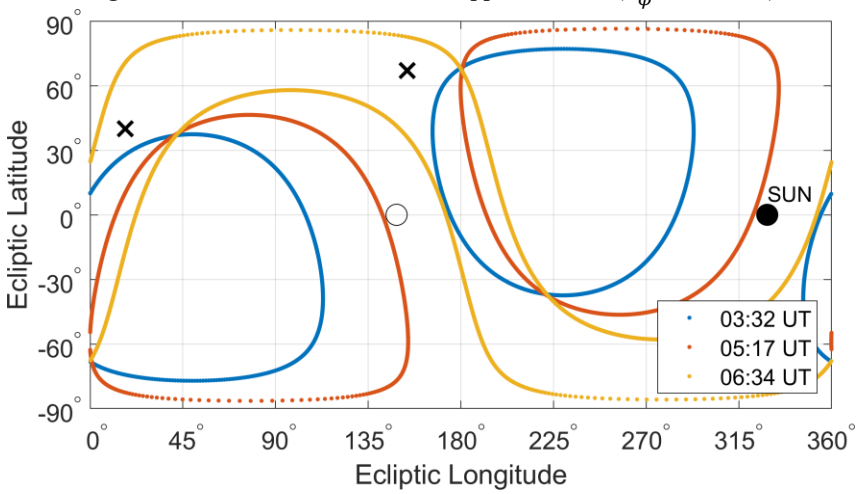

Fig. 15: Feb. 18, 2020 GOES 10 Candidate Poles in the J2000 Ecliptic Frame.

4.3 GOES 11

GOES 11 Doppler echoes obtained on Dec. 6, 2019 are provided in Figure 16. Phase-folding the echoes indicated $P_{\bar{\phi}}^{syn}$ = 775 s (12.9 min). Comparing the top and bottom plots in Figure 16, we see significant change in Doppler bandwidth over the three hour observation span. Photometry collected on Dec. 17, 2019 did not fold cleanly on any candidate rotation period, indicating non-principal axis rotation. Given only 11 days between collection of the photometry and radar, it is very likely that GOES 11 was also tumbling on Dec. 6. Lomb-Scargle analysis, used in lieu of FFT analysis due to significant observation gaps, suggested $P_{\bar{\phi}}^{syn} \sim$ 13 min. This value is comparable to that obtained from our radar observations 11 days prior. Approximating GOES 11 in uniform rotation (given that $\dot{\phi}$ is almost constant for the nearly axisymmetric GOES satellites) and computing the Doppler bandwidth and 2D RPD pole estimates, the resulting solutions are provided in Figure 17. The 2D RPD solutions are in the vicinity of two Doppler bandwidth solutions. These combined solutions place the pole within ~ 45° of the sun/anti-sun directions.

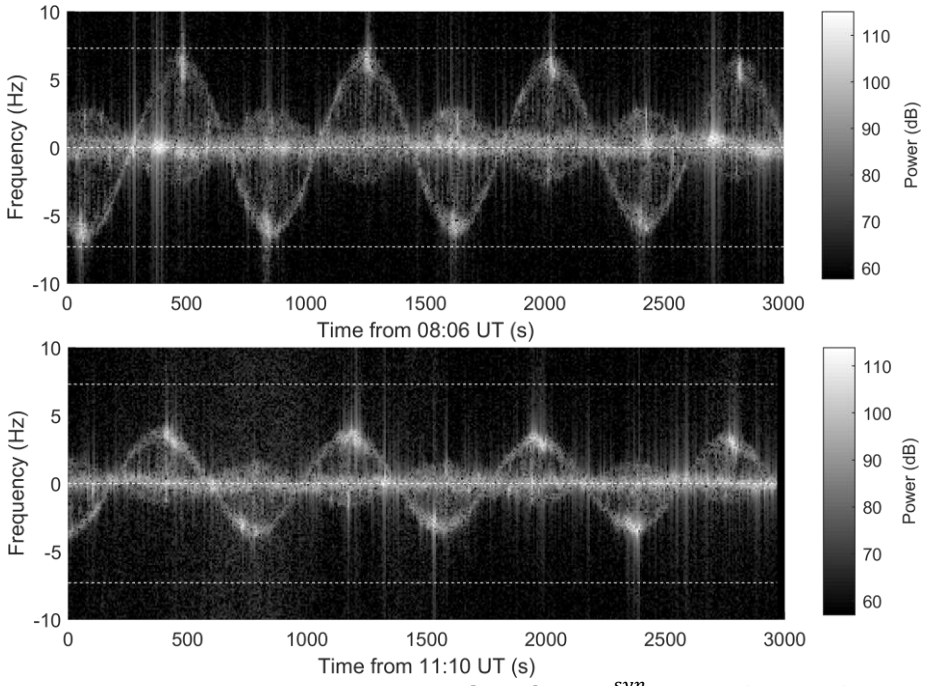

Fig. 16: Dec. 6, 2019 GOES 11 Doppler Echoes. $P_{\bar{\phi}}^{syn}$ = 775 s (12.9 min).

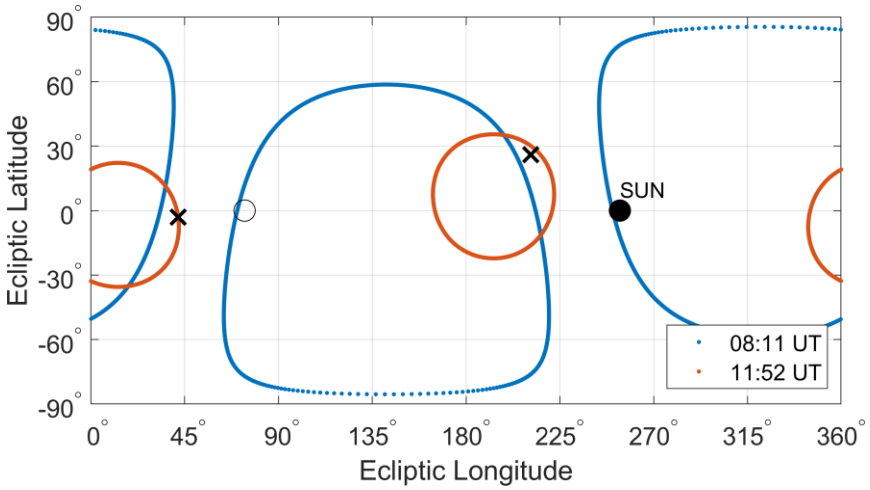

Fig. 17: Dec. 6, 2019 GOES 11 Candidate Poles in the J2000 Ecliptic Frame.

4.4 GOES 12

GOES 12 was observed on Dec. 6, 2019 and Feb. 18-20, 2020. The Dec. 6 echoes indicated $P_{\bar{\phi}}^{syn} = 882$ s (14.7 min). The February 18-20 echoes indicated $P_{\bar{\phi}}^{syn}$ decreasing from 462 s (7.7 min) to 454 s (7.6 min). Photometry collected from February 18-20 at Magdalena Ridge Observatory indicated GOES 12 was in uniform rotation. So the satellite was likely uniformly rotating on Dec. 6 as well. Calculating the Doppler bandwidth and 2D RPD pole estimates, the resulting solutions on Dec. 6, 2019 and Feb. 20, 2020 are provided in Figures 18 and 19. The December solutions indicate the pole is below the ecliptic plane with $\delta \sim$ -45°. Continuing to February 20, the closest solution and therefore most likely, has $\lambda \sim$ 265° and $\delta \sim$ -70°. The two candidate poles on February 18, 2020 were virtually identical to those from February 20.

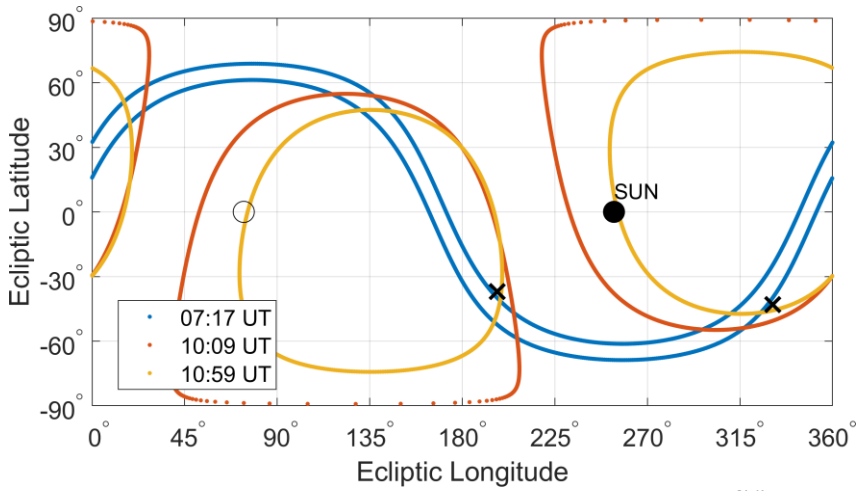

Fig. 18: Dec. 6, 2019 GOES 12 Candidate Poles in the J2000 Ecliptic Frame. $P_{\bar{\phi}}^{syn}$ = 882 s (14.7 min).

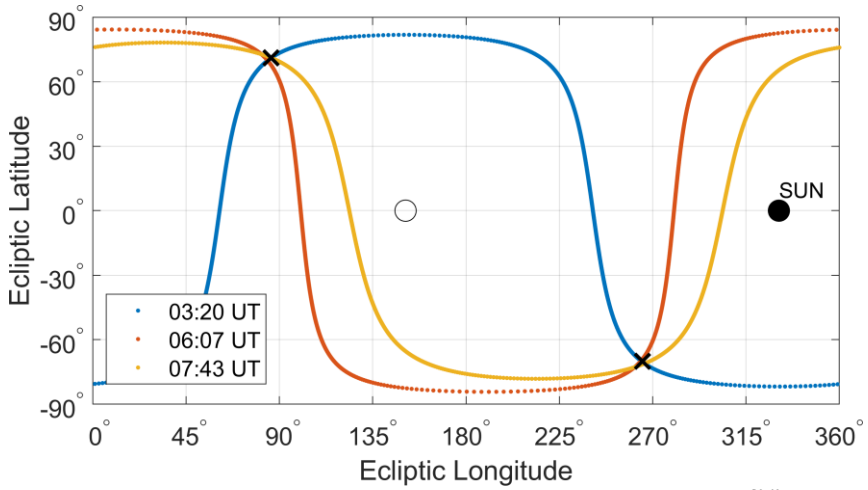

Fig. 19: Feb. 20, 2020 GOES 12 Candidate Poles in the J2000 Ecliptic Frame. $P_{\bar{\phi}}^{syn}$ = 454 s (7.6 min).

5. DISCUSSION

The most obvious takeaway from the above analysis is the spin state diversity of these four GOES satellites. Table 2 summarizes the $P_{\bar{\phi}}$ estimates obtained above. GOES 8 and GOES 11 were in slow non-principal axis rotation while GOES 12 was in slow uniform rotation. GOES 10 on the other was in fast uniform rotation with a ~30 s precession period, a state is has maintained since at least 2014 [2,7]. Overall, this large spin state diversity further supports the idea that the end of life solar panel angles of the GOES satellites (which differ greatly) largely dictate their long-term evolution. Previously, we found that the known end of life solar panel angle of GOES 10 nearly minimizes

solar radiation torques, while the angles for the remaining four satellites GOES 8, 9, 11 and 12 leave them much more susceptible to the YORP effect [7]. This continues to be supported by observations. Furthermore, this illustrates the potential for carefully setting end of life solar panel angles to minimize long-term spin rate evolution, facilitating active debris removal and satellite servicing. Another trend we saw was that the tumbling satellites, name GOES 8 and GOES 11, had candidate poles significantly closer to the sun/anti-sun directions than the uniform rotators GOES 10 and GOES 12. This is also consistent with YORP theory since we have found that the poles of tumbling satellites tend to track and precess about the sun/anti-sun directions [8,9].

Table 2: Summary of GOES $P_{\bar{\phi}}$ Estimates (* denotes tumbling)

	GOES 8	GOES 10	GOES 11	GOES 12
Dec. 6, 2019	*353 s (5.9 min)	-	*775 s (12.9 min)	882 s (14.7 min)
Feb. 18, 2020	*215 s (3.58 min)	30.5 s	-	462 s (7.7 min)
Feb. 20, 2020	*216 s (3.6 min)	30.5 s	-	454 s (7.6 min)

Table 2 also illustrates the pronounced changes in precession periods for GOES 8 and GOES 12, with periods decreasing by almost 50% in 2.5 months. Their candidate pole directions changed significantly as well. This demonstrates that more observation and modeling is needed to understand and predict the ongoing evolution of these spin states. Of particular interest for our ongoing dynamical studies is GOES 8's apparent 5:1 tumbling period resonance observed on February 18, 2020. Intriguingly, this is the same resonance observed in April 2018, albeit with $P_{\bar{\phi}}$ ~ 293 s (4.88 min) [5]. YORP Dynamical simulations of the GOES satellites have also shown such tumbling period resonances with $P_{\psi}/P_{\bar{\phi}}$ = 1,2 being most common [8,9]. In these resonances, the satellite's two tumbling periods vary together while remaining in lock step and maintaining the resonance for an extended period of time. Furthermore, the 5:1 resonance observed in 2018 and 2020 puts GOES 8 near the separatrix (the curves that separate regions of $\vec{\omega}$ circulation around the minimum and maximum inertia axes) [5]. Simulating YORP with internal energy dissipation (e.g. from fuel slosh or flexible structures), we found that the GOES satellites often settled into stable tumbling states near the separatrix with constant $P_{\bar{\phi}}$, P_{ψ} values and the angular momentum vector (pole) fixed in the sun-satellite rotating orbit frame [8]. The fact that GOES 8's precession period changed across the 2018, 2019, and 2020 observations indicates it is not in a stable tumbling state. A possible explanation for this is gravity gradient torques from earth which generally cause the satellite's pole to precess about its GEO orbit normal direction, potentially perturbing or destroying such stable tumbling states.

Comparing the radar-derived precession period for GOES 8 on Feb. 18, 2020 to the significant MRO light curve frequencies, we found that the primary light curve frequency is $2f_{\bar{\phi}}$ and all other prominent frequencies were low order harmonics of $f_{\bar{\phi}}$ and f_{ψ}. This observationally confirms our simulation findings from [5] that multiples of $f_{\bar{\phi}}$ dominate the light curve structure for GOES and that all significant frequencies are directly related to the two tumbling periods. Overall, these findings increase our confidence in identifying the dominant light curve frequencies for GOES and other tumbling satellites.

6. CONCLUSIONS

Overall, we developed and applied Doppler radar spin state estimation techniques that greatly aid in satellite spin state estimation. Unlike light curves, Doppler provides spatial resolution due to satellite rotation. This allows for clear identification of spacecraft features. Furthermore, Doppler vastly simplifies pole estimation as well as precession period extraction in the tumbling case. For 3D Rotationally Phased Doppler, precise spin period and pole estimates can be obtained without a detailed spacecraft model, provided significantly non-planar viewing geometry and a fixed spin state. This is a huge improvement over light curve based inversion where accurate, high fidelity spacecraft models are often needed to replicate the observed specular reflections and glints.

Applying these radar-based estimation techniques, we obtained unambiguous precession periods for both tumbling and uniformly rotating GOES satellites. Leveraging near-simultaneous light curve observations, we also determined the second tumbling period for GOES 8. The radar analysis also greatly constrained the possible pole directions. We found large diversity in precession periods and pole directions among the nearly identical GOES satellites with notable evolution over a 2.5 month span for GOES 8 and GOES 12. This spin state diversity and evolution is consistent with YORP-driven behavior. Furthermore, the rich diversity, pole motion, and tumbling resonances observed for these satellites motivates further observations and dynamical study.

ACKNOWLEDGEMENTS

This work was supported by a NASA Space Technology Research Fellowship and Jet Propulsion Laboratory R&TD innovative spontaneous concepts proposal. The primary author would like to thank Razi Ahmed at the Jet Propulsion Laboratory for fruitful discussion about radar interferometry.

REFERENCES

[1] Papushev, P., Karavaev, Y., Mishina, M., Investigations of the evolution of optical characteristics and dynamics of proper rotation of uncontrolled geostationary artificial satellites, *Advances in Space Research*, Vol. 43, pp. 1416–1422, 2009.

[2] Cognion, R. L., Rotation rates of inactive satellites near geosynchronous earth orbit, *Proceedings of AMOS 2014.*

[3] Ryan, W. H., Ryan, E. V., Photometric Studies of Rapidly Spinning Decommissioned GEO Satellites, *Proceedings of AMOS 2015*.

[4] Earl, M. A., Wade, G. A., Observations of the Spin-Period Variation of Inactive Box-Wing Geosynchronous Satellites, *Journal of Spacecraft and Rockets*, Vol. 52(3), pp. 968–977, 2015.

[5] Benson, C. J., Scheeres, D. J., Ryan, W. H., Ryan, E. V., Cyclic complex spin state evolution of defunct GEO satellites, *Proceedings of AMOS*, 2018.

[6] Albuja A. A., Scheeres, D. J., Cognion, R. L., Ryan, W., Ryan, E. V., The YORP effect on the GOES 8 and GOES 10 satellites: A case study, *Advances in Space Research*, Vol. 61, pp. 122-144, 2018.

[7] Benson, C. J., Scheeres, D. J., Ryan, W. H., Ryan, E. V., Moskovitz, N. A., GOES Spin State Diversity and the Implications for GEO Debris Mitigation, *Acta Astronautica*, Vol. 167, pp. 212-221, 2020.

[8] Benson, C. J., Scheeres, D. J., The YORP Effect for Tumbling Defunct GEO Satellites (AAS 19-858), Proceedings of the AAS/AIAA Astrodynamics Specialist Conference, Portland, ME, 2019.

[9] Benson, C. J., Scheeres, D. J., Averaged Solar Torque Rotational Dynamics for Defunct Satellites, *Journal of Guidance, Control, and Dynamics*, in review.

[10] Rubincam, D., Radiative spin-up and spin-down of small asteroids, *Icarus*, Vol. 148, pp. 2-11, 2000.

[11] *GOES I-M Databook*, Rev. 1, Aug. 31, 1996, https://goes.gsfc.nasa.gov/text/goes.databook.html, retrieved Sept. 9, 2017.

[12] Pravec, P., et al., Tumbling Asteroids, *Icarus*, Vol. 173(1), 108-131, 2005.